Journal of large-scale research facilities

Journal of large-scale research facilities, 3, A112 (2017) http://dx.doi.org/10.17815/jlsrf-3-158

Published: 22.05.2017

HNF - Helmholtz Nano Facility

Forschungszentrum Jülich GmbH *

Head:
- Dr. Wolfgang Albrecht, Helmholtz Nano Facility, Jülich Research Centre, 52425 Jülich, Germany, phone: ++49 2461 61 6364, e-mail: w.albrecht@fz-juelich.de

Officer Technology Section I:
- Dr. Jürgen Moers, Helmholtz Nano Facility, Jülich Research Centre, 52425 Jülich, Germany, phone: ++49 2461 61 2344, e-mail: j. moers@fz-juelich.de

Officer Technology Section II:
- Dipl. Ing. Bernd Hermanns, Helmholtz Nano Facility, Jülich Research Centre, 52425 Jülich, Germany, phone: ++49 2461 61 3193, e-mail: be.hermanns@fz-juelich.de

Abstract: The Helmholtz Nano Facility (HNF) is a state-of-the-art cleanroom facility. The cleanroom has ~1100 m^2 with cleanroom classes of DIN ISO 1-3. HNF operates according to VDI DIN 2083, Good Manufacturing Practice (GMP) and equivalent to Semiconductor Industry Association (SIA) standards. HNF is a user facility of Forschungszentrum Jülich and comprises a network of facilities, processes and systems for research, production and characterization of micro- and nanostructures. HNF meets the basic supply of micro- and nanostructures for nanoelectronics, fluidics. micromechanics, biology, neutron and energy science, etc..

The task of HNF is rapid progress in nanostructures and their technology, offering efficient access to infrastructure and equipment. HNF gives access to expertise and provides resources in production, synthesis, characterization and integration of structures, devices and circuits. HNF covers the range from basic research to application oriented research facilitating a broad variety of different materials and different sample sizes.

1 Access to HNF

HNF is a user facility according to HGF infrastructures and proposal based. Evaluations of proposals are done by a scientific/technical board. Access, safety management and tool booking is done via a professional web based managing platform. This is a combination of web presence (www.hnf.fz-juelich.de)

* **Cite article as:** Forschungszentrum Jülich GmbH . (2017). HNF - Helmholtz Nano Facility. *Journal of large-scale research facilities, 3*, A112. http://dx.doi.org/10.17815/jlsrf-3-158

and manufacturing execution system (MES).
HNF is organized by the HNF Office. It is the first contact for users in scientific and technical matters. HNF Office organizes the application process, the acceptance of applications for scientific projects and the assessment of their scientific and technical feasibility. The HNF Office implements the recommendations of the HNF steering committee. It coordinates the work of HNF.

2 Overview of technologies

The technology platform of HNF provides a wide range of standard planar technologies:

2.1 Pattern Definition:

For pattern definition Electron-Beam-Lithography, Nanoimprint-Lithography and optical Lithography are used:

Type	Tool	Description
Electron-Beam Lithography	Vistec EBPG 5000+	50/100keV, up to 150 mm, overlay 0.5nm±2.5nm
Optical Lithography	Süss MA/BA8Gen3	front and backside alignment; ~0.3 μm MFS; overlay 0.25μm; up to 200 mm
	Süss MA 6	front and backside alignment; ~0.3 μm MFS; overlay ~1 μm; up to 150 mm
	Süss MA 4	front and backside alignment; ~1 μm MFS; overlay ~1 μm; up to 100 mm
	Süss MA 4	front and backside alignment; ~1 μm MFS; overlay ~1 μm; up to 100 mm
Nano-Imprint	Nanonex NX-2000	Up to 100 mm; 30 nm MFS; overlay (via Süss MA6) ~1 μm

2.2 Pattern transfer:

Pattern transfer by dry etching is done in 8 etching chambers, one in RIE, 6 in RIE/ICP and one in PE mode; the large number of etching chambers is due to the large variety of different materials:

Type	Tool	Description
Dry Etching	Oxford PLS 100 RIE/ICP cluster tool	Up to 150 mm, load lock Chamber 1: RIE, Gas species: Ar, O_2, SF_6, CHF_3, C_4F Chamber 2: ICP Gas species: Ar, O_2, HBr, Cl_2
	Oxford PLS 100 ICP cluster tool	Up to 200 mm, load lock, only CMOS Chamber 1: ICP, Gas species: Ar, O_2, SF_6, CHF_3, CF_4 Chamber 2: ICP, Gas species: Ar, O_2, HBr, Cl_2
	Oxford PLS 100 ICP	Up to 150 mm, load-lock, Gas species: Ar, O_2, CF_4, Cl_2, HBr,
	Oxford PLS 100 ICP	Up to 150 mm, load lock, only Si based materials Gas species: Ar, O_2, H_2, S_6, CHF_3, Cl_2, C_4F_8; Bosch and Cryo process for deep silicon etching
	Oxford PLS 100 ICP	Up to 150 mm, load lock, Gas species: Ar, O_2, CF_4, Cl_2, HBr
	TePla Gigabatch 360 plasma etcher	Resist stripping, N_2, O_2, CF_4, up to 150 mm

2.3 Layer Deposition:

Besides e-beam- and sputter deposition of metals, CVD systems for dielectrics and SiGe-epitaxy, ALD systems for high-κ-materials and AVD systems for metal gate like TiN, TaN and AlN are applicable:

Type	Tool	Description
Physical vapor deposition	Balzers PLS 500	Up to 3 x 100 mm wafers, load lock, Ar-cleaning, 6 crucibles, different metals
	Balzers PLS 570	Up to 5 x 150 mm, load lock, Ar - Cleaning, 6 crucibles, Al, Au, Ti, Pt, Ag und Cr, for Bio-inspired systems
	Leybold Univex400	Up to 100 mm, Ar-Cleaning, 8 crucibles
	Oerlikon Evo2	Up to 200 mm, CMOS only DC/RF-Sputtering, three sources parallel, Al, Ti, TiN, Ta, Ni, TaN, Insulators
CVD/ALD/VPE	Oxford PLS 100 PECVD	up to 200 mm, load lock, SiO_2, SiN_x; LR- and RF-plasma modes
	Sentech PECVD Si 500 PPD	Up to 200 mm, load lock, SiO_2, SiN_x, low temperature deposition (100°C < T < 350°C)
	Oxford ALD	Up to 150 mm, TaO_xx, SiN_x
Aixtron Tricent Cluster	Aixtron Tricent Cluster CVD	SiGe epitaxy for 300mm
	Aixtron Tricent Cluster CVD	SiGeSn epitaxy for 200mm
	Aixtron Tricent Cluster ALD	High-k, HfO_2, Al_2O_3, $Hf_yAl_{(1-y)}O_x$ wafers 300 mm, 200 mm, 100 mm; pieces 19.5 mm x 19.5 mm
	Aixtron tricent Cluster AVD	Metal gate AVD, TiN, TaN; wafers 300 mm, 200 mm, 100 mm; pieces 19.5 mm x 19.5 mm

2.4 Chemical treatment and resist technology:

Four wet bench lines are located at HNF to provide resist technologies for the different material systems and means for wet chemical treatment of samples:

Type	Tool	Description
Wet Benches	Full wet bench line for Si processing	Wet benches for Preclean, Cleaning S1/S2, RCA, Resist, coating (incl. HDMS), Development, Solvents, Lift off, wet etching, up to 200 mm
	Full wet bench line for III/V processing	Wet benches for Preclean, Cleaning, Resist coating (incl. HDMS), Development, Solvents, Lift off, wet etching, up to 150 mm
	Full wet bench line for Biohybrids and not semiconductor materials	Wet benches for Preclean, Cleaning, Resist coating (incl. HDMS), Development, Solvents, Lift off, wet etching, up to 200 mm

	Four Wet benches for Precleaning and Etching of "special materials"	Two benches for cleaning and etching with acids and bases, Two wet benches for handling solvents, up to 200 mm
	Wet bench mask making of chromium masks	Two wet benches for developing and etching chromium masks, up to 200 mm
Wafer Cleaner	SSEC wafer cleaner	1 reactor, up to 150 mm; Si-based materials
	Semitool wafer cleaner	2 reactors for 200 mm and 2 reactors for 300 mm
	SemiSolar mask cleaner	for mask up to 5”
Critical point dryer	Tousimis® 931 series	Up to 2.5”

2.5 Ion implantation

Three ion implanters varying in samples size and energy range are operated:

Type	Tool	Description
Implanter	Axcelis Optima HDX	Up to 300 mm, 200ev-60Kev, B, BF_2, P, As, Si, H, H_2
	Axcelis 8250 Eaton NV 3204	Up to 150 mm, 1 KeV- 250 KeV B, BF_2, P, As, Si, H, Up to 100 mm, 20-200 KeV

2.6 Thermal processing

Rapid Thermal Processing (RTP) and thermal diffusion furnaces varying in sample size and allowed material classes:

Type	Tool	Description
Rapid Thermal Processing	UniTemp RTP 150	Rapid Thermal Processing for Si, SiGe Gas species: N_2, H_2, O_2, Ar, max 1000°C, up to 100 mm
	UniTemp RTP 150	Rapid Thermal Processing for III/V Gas species: N_2, H_2, O_2, Ar, max 1000°C, up to 100 mm
	Mattson Helios RTP	Dual Chamber for Si, SiGe, SiGeSn, CMOS, wafers 300mm, 200mm, 100mm, pieces 19,5mm*19,5mm Gas species: N_2, forming gas: Ar, O_2, Min: 300°C; max 1100°C Spike, soak classes
	Mattson ST 2000 RTP	for 150 mm Si,
	Steag ST 2000 RTP	Rapid Thermal Processing for Si; Gas species: N_2O, O_2, H_2, Ar, N_2, max 1050°C, up to 150 mm
Diffusion furnaces	Tempress, horizontal furnace	Wet and dry thermal oxidation of Si; up to 100 mm; T: 800 - 1100 °C
	Tempress, horizontal furnace	Wet and dry thermal oxidation of Si and metals; up to 100 mm; T= 450 - 1100 °C

	Tempress, horizontal furnace	Dry thermal oxidation of Si; up to 100 mm; T = 800 - 1100 °C
	Centrotherm CLV, Vertical Furnace	up to 200 mm: N_2, N_2O, H_2O, O_2, DCE, max. 1050°C
	Centrotherm CLV, Vertical Furnace	up to 200 mm: N_2, H_2O, O_2, DCE, max. 1050°C

2.7 Analysis

HNF limits the analysis tools in house, but has access to a lot of tools like Rutherford Backscattering, Atomprobe, Hall Measurement, SIMS, Photoluminescence, etc.

Type	**Tool**	**Description**
Electron Microscopy	FEI Magellan , SEM	High resoluition SEM for electron energies below 5 KeV, Energy dispersive X-ray analysis
	FEI Helios FIB + EBID	Focused Ion Beam, EBID for PT, Au, SiO_2, Ir, Cryo stage for biological applications
	Zeiss 1550 SEM	General purpose SEM, Gemini column, 30keV
	Zeiss 1550 VP SEM	General purpose SEM, Gemini column, 30keV
Ellispometry	SENTECH SE800 spectroscopic ellipsometer	Up to 300 mm, mapping
Profilometry	Bruker Dektak 150, Surface profiler	2 nm vertical resolution
Atomic Force Microscopy	Bruker SIS-AFM	Up to 100 mm;
Optical Microscopy	Leitz INM 100	Optical microscope
	Leitz INM 300	UV-optical microscope

2.8 Dicing

One semi-automatic wafer dicer and two manual systems are operated to singularize chips:

Type	**Tool**	**Description**
Dicing	Disco DAD3350.	Si, glass, Al_2O_3, ceramics, up to 200 mm and thickness of 1.5mm; no III/V-materials
	Süss Scriber	Up to 100 mm, for Si
	Süss Scriber	Up to 100 mm

3 Examples of Applications

3.1 Quantum Information

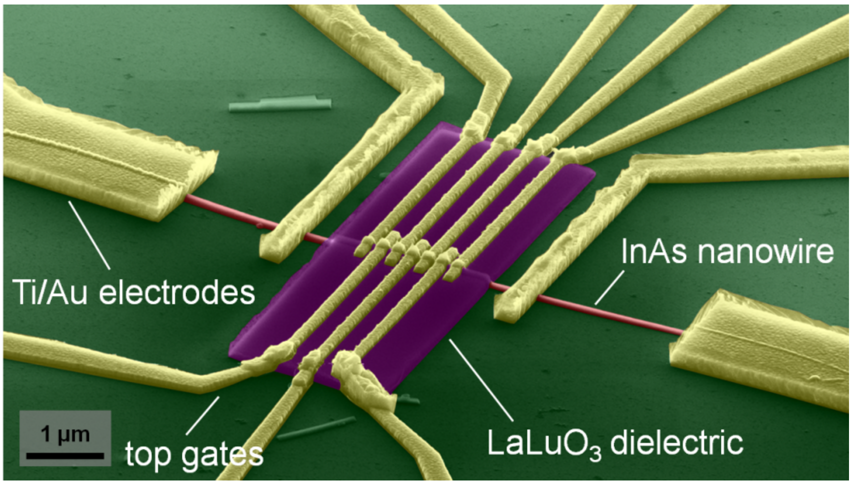

Figure 1: Gated Nanowire Mulitple Quantum Point Device (Heedt et al., 2016)

Figure 1 shows a scanning electron micrograph of an InAs nanowire (diameter 100 nm) investigated in (Heedt et al., 2016). It is partially covered with 100 nm of the high-k dielectric $LaLuO_3$ (ε_r= 26.9). Hence, each top-gate electrode is coupled stronger to the nanowire than the back gate. The seven top gate electrodes each have a width of 180 nm, and the gate pitch is 30 nm. The back gate and each top gate can be used to pinch-off the channel completely and control the number of subbands contributing to transport.

3.2 Nanoelectronics

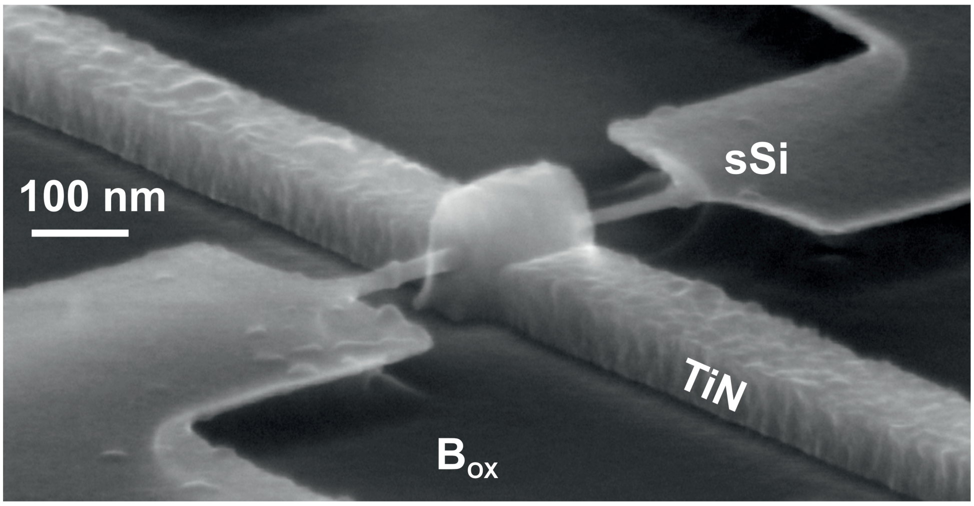

Figure 2: Complementary strained Si GAA Nanowire TFET with suppressed ambipolarity nanowire transisto (Luong et al., 2016).

In Figure 2 complementary tunneling field-effect transistors (CTFETs) based on strained Si with gate all around nanowire structures on a single chip is shown. The main focus is to suppress the ambipolar behavior of the TFETs with a gate–drain underlap. Detailed device characterization and demonstration of a CTFET inverter show that the ambipolar current is successfully eliminated for both p- and n-devices. The CTFET inverter transfer characteristics indicate maximum separation of the high/low level with a sharp transition (high voltage gain) at a V_{dd} down to 0.4 V. In addition, high noise margin levels of 40% of the applied V_{dd} are obtained (Luong et al., 2016).

3.3 MEMS

Figure 3 shows (a) a schematic illustration of microelectromechanical actuator. The red arrow indicates the lateral vibration of a silicon beam. Scanning electron microscope (SEM) images of (b) the comb-drive actuator and (c) a zoom in the dashed red box in panel (b). The scale bars indicate 20 μm and 2 μm, respectively. The electronic circuit depicted in (d) is used to measure the resonance frequency, where the inner green box indicates the device and the red box indicates the printed circuit board (PCB) in the cryostat at T = 2.3K. An AC signal ($V_{sd}(f\text{-}\Delta f)$) drives the current from source (S) to drain (D) contact, while a sum of DC and AC voltages ($V_{sg} + V_{sg}^{AC}(f)$) are applied to the side-gate (SG). The down-mixed current at frequency Δf through the resonator is measured by an I/V-converter and a lock-in amplifier. The comb-drive actuator is driven by a DC voltage Vcd. The capacitors C_0 = 100 nF and resistors R_0 = 50 Ω are chosen for impedance matching and decoupling any high frequency signals.

3.4 Microfluidic

Figure 4 shows a fabricated microfluidic chip device with picolitre bioreactors (PLBR) for cultivation and investigation of bacteria on the single cell level Grünberger et al. (2012). (A) The PDMS microfluidic chip was bonded to a 170 mm glass slide and connected to silicone tubing. For purpose of illustration, the chip was filled with ink. Each chip is 4 mm *x* 15 mm *x* 20 mm (height *x* width *x* length) in size. The device consists of two inlets, one outlet, a microfluidic gradient generator for future studies and 6 linear arrays containing 5 PLBRs each (30 PLBRs in total). (B) CAD image of one PLBR array, containing 5 PLBRs in parallel. (C) SEM of a single PLBR with 1 pL cultivation volume. The height of the PLBR is approx. 1 mm and the supply channel height is approx. 10 mm. Seeding and overflow channels have a width of 2 mm.

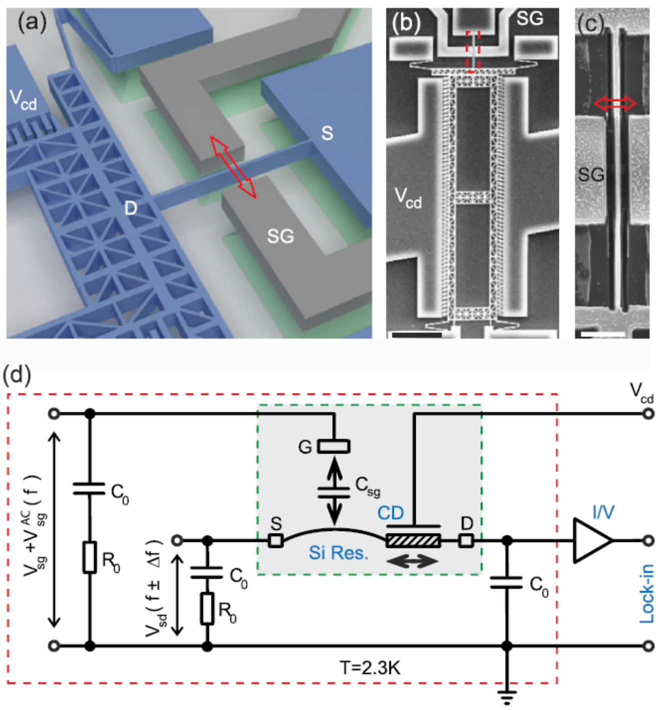

Figure 3: Tunable mechanical coupling between driven microelectromechanical resonators.

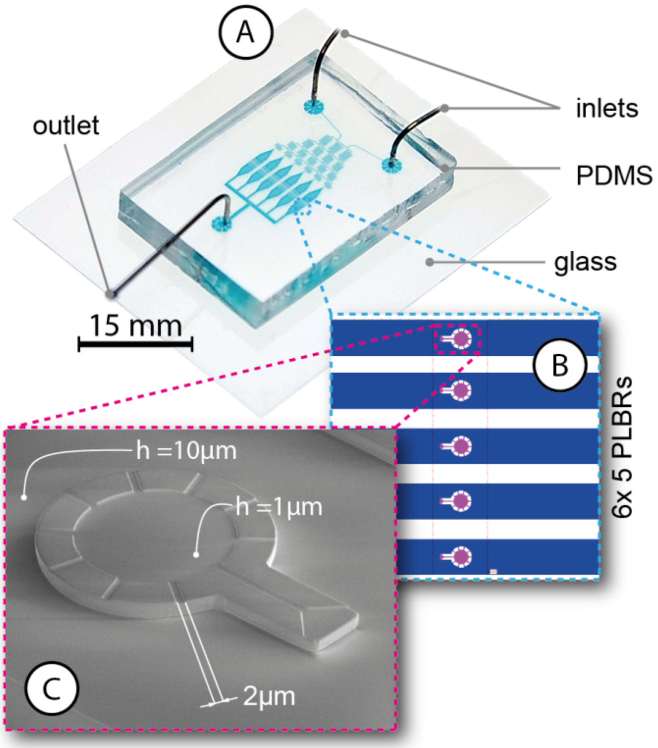

Figure 4: Microfluidic chip device with picolitre bioreactors for single cell cultivation.

3.5 Biosensors

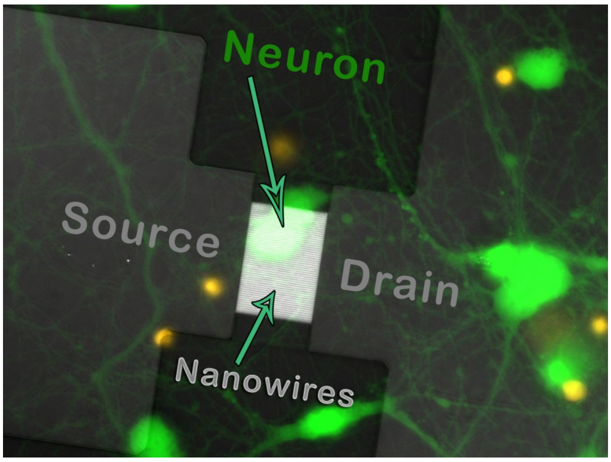

Figure 5: Double-gated Si NW FET sensor [6] (Gasparyan et al., 2016)

Figure 5 shows double gates Si NW FET arrays for biological signal detection. The transport, noise, and photosensitivity properties of an array of silicon nanowire (NW) p++-p-p+ field-effect transistors (FETs) shows an shift of absorbance of p-Si NW to the short wavelength region compared with bulk Si. Sensitivity values can be tuned by the drain-source voltage and may reach record values of up to 2-4 A/W. The drain current of Si NW biochemical sensors substantially depends on pH value and the signal-to-noise ratio reaches the high value of 105. Increasing pH sensitivity with gate voltage is revealed for certain source-drain currents of pH-sensors based on Si NW FETs. The noise characteristic index decreases from 1.1 to 0.7 with the growth of the liquid gate voltage. Noise behavior is successfully explained in the framework of the correlated number-mobility unified fluctuation model. pH sensitivity increases as a result of the increase in liquid gate voltage, thus giving the opportunity to measure very low proton concentrations in the electrolyte medium at certain values of the liquid gate voltage (Gasparyan et al., 2016).

References

Gasparyan, F., Khondkaryan, H., Arakelyan, A., Zadorozhnyi, I., Pud, S., & Vitusevich, S. (2016). Double-gated si nw fet sensors: Low-frequency noise and photoelectric properties. *Journal of Applied Physics*, *120*(6), 064902. http://dx.doi.org/10.1063/1.4960704

Grünberger, A., Paczia, N., Probst, C., Schendzielorz, G., Eggeling, L., Noack, S., … Kohlheyer, D. (2012). A disposable picolitre bioreactor for cultivation and investigation of industrially relevant bacteria on the single cell level. *Lab Chip*, *12*, 2060-2068. http://dx.doi.org/10.1039/C2LC40156H

Günel, H. Y., Borgwardt, N., Batov, I. E., Hardtdegen, H., Sladek, K., Panaitov, G., … Schäpers, T. (2014). Crossover from Josephson Effect to Single Interface Andreev Reflection in Asymmetric Superconductor/Nanowire Junctions. *Nano Letters*, *14*(9), 4977-4981. http://dx.doi.org/10.1021/nl501350v

Heedt, S., Prost, W., Schubert, J., Grützmacher, D., & Schäpers, T. (2016). Ballistic Transport and Exchange Interaction in InAs Nanowire Quantum Point Contacts. *Nano Letters*, *16*(5), 3116-3123. http://dx.doi.org/10.1021/acs.nanolett.6b00414

Kireev, D., Seyock, S., Ernst, M., Maybeck, V., Wolfrum, B., & Offenhäusser, A. (2017). Versatile Flexible Graphene Multielectrode Arrays. *Biosensors*, *7*, 1. http://dx.doi.org/10.3390/bios7010001

Luong, G. V., Narimani, K., Tiedemann, A. T., Bernardy, P., Trellenkamp, S., Zhao, Q. T., & Mantl, S. (2016). Complementary Strained Si GAA Nanowire TFET Inverter With Suppressed Ambipolarity. *IEEE Electron Device Letters*, *37*(8), 950-953. http://dx.doi.org/10.1109/LED.2016.2582041

Pud, S., Li, J., Sibiliev, V., Petrychuk, M., Kovalenko, V., Offenhäusser, A., & Vitusevich, S. (2014). Liquid and Back Gate Coupling Effect: Toward Biosensing with Lowest Detection Limit. *Nano Letters*, *14*(2), 578-584. http://dx.doi.org/10.1021/nl403748x

Verbiest, G. J., Xu, D., Goldsche, M., Khodkov, T., Barzanjeh, S., von den Driesch, N., … Stampfer, C. (2016). Tunable mechanical coupling between driven microelectromechanical resonators. *Applied Physics Letters*, *109*(14), 143507. http://dx.doi.org/10.1063/1.4964122